Nanoscale

PAPER

View Article Online
View Journal | View Issue

Cite this: *Nanoscale*, 2024, **16**, 15824

Tailoring electrochemically exfoliated graphene electroactive pathways in cementitious composites for structural health monitoring of constructions

Małgorzata Safuta, *[a] Cataldo Valentini, [b] Artur Ciesielski [b,c] and Paolo Samorì *[c]

Manipulating and exerting a nanoscale control over the structure of multicomponent materials represents a powerful strategy for tailoring multifunctional composites for structural health monitoring applications. The use of self-sensing, electroactive cementitious composites in large-scale applications is severely hindered by the absence of clear directives and a thorough understanding of the electrical conduction mechanisms taking place within the cement matrix. Here we report on a nanoscale approach towards this goal which is accomplished *via* the development of a novel, multifunctional cementitious composite incorporating electrochemically exfoliated graphene (EEG). The use of commercially available poly(carboxylate ether)-based superplasticizer allowed us to embed in the cement mortar up to 0.8 wt% of EEG which is fully dispersed in the matrix. The multiscale investigation made it possible to assess the effect of such high dosages of EEG on the mechanical performance and hydration degree of cementitious composites. We used electrochemical impedance spectroscopy to monitor the formation of electroactive EEG-based percolation paths for charge transfer within cement mortar, the latter displaying resistivities of 2.67 kΩ cm as well as EEG-cement-EEG capacitive paths with capacitance of 2.20 × 10^{-10} F cm^{-1} for composites incorporating 0.6 wt% of EEG. Noteworthy, we have proposed here for the first time an electrical equivalent circuit for the impedance spectroscopy analysis of cementitious composites with high loadings of graphene, exceeding the percolation threshold. These findings underscore the potential of nanoscale structures for civil engineering applications and more specifically may open new avenues for the technological application of graphene-based cementitious composites in self-sensing structures.

Received 23rd April 2024,
Accepted 5th August 2024

DOI: 10.1039/d4nr01764a

rsc.li/nanoscale

Introduction

The durability, sustainability and safety of modern building structures increasingly rely on Structural Health Monitoring (SHM) which takes place through the continuous, real-time measurements of the structural response to external loads and/or weather conditions, enabling the immediate noticing of damage occurrence.[1,2] Over the past decades, self-sensing cementitious composites have attracted considerable attention in the field of SHM as materials overcoming the commonly existing limitations in external sensors, such as low durability and compatibility with concrete structure, high cost or the need of extensive connections and equipment.[1–4] Self-sensing cementitious composites are manufactured by incorporating conductive functional nanofillers that may transform an electrically insulating cementitious composite into a multifunctional sensor acting simultaneously as a high-performance structural material. With the introduction of functional (nano) fillers forming electroactive paths within cement matrix, the novel material becomes capable of detecting stress, strain or cracks due to the changes of electrical parameters such as resistivity, capacitance, impedance, dielectric constant *etc.*[2–5] The most studied functional fillers in self-sensing concrete are based on steel and carbon fibres, carbon black, graphite and carbon nanotubes.[2,4,6–10] Unfortunately their implementation in real-scale structures is still precluded due to the broadest diversity of reported results. This is due to the fact that the properties of self-sensing concrete are strongly affected by the type and morphology adopted by the functional fillers as well as by their alignment and dispersion within the cement matrix.[11,12] Therefore, the search for the novel materials

[a]*Department of Structural Engineering, Silesian University of Technology, Akademicka 5, 44-100 Gliwice, Poland. E-mail: malgorzata.safuta@polsl.pl*
[b]*Centre for Advanced Technologies, Adam Mickiewicz University, Uniwersytetu Poznańskiego 10, 61-614 Poznań, Poland*
[c]*Université de Strasbourg, CNRS, ISIS, 8 allée Gaspard Monge, 67000 Strasbourg, France. E-mail: samori@unistra.fr*

offering a high-control over the electrical properties of cementitious composites represents a key step for the development of self-sensing concrete. Noteworthy, graphene's outstanding properties[7,13–15] make it one of the most promising nanomaterials for application in composites, including civil engineering applications, with the ultimate goal of designing high-performance, self-monitoring structures. Among various synthesis protocols, electrochemical exfoliation of graphite offers the possibility to obtain graphene flakes of different sizes, thicknesses and quality, together with enabling the production of high quantities of graphene at industrial scale with high efficiency, at low cost, and in an environmentally friendly manner.[16,17] Moreover, as reported in our previous studies,[18,19] the addition of low dosages of electrochemically exfoliated graphene (EEG) proved to be greatly beneficial for the cement hydration, the development of the microstructure of cement-based composites as well as for their mechanical and durability-related properties. Therefore, considering also its excellent electrical properties,[16,20] EEG is emerging as an attractive functional filler for self-sensing applications in concrete structures.

Importantly, the findings reported in the literature[11,21,22] highlight the greatest challenge in the field of self-sensing cementitious composites being the development of the reproducible, precise and easy applicable methods for elucidating the electrical properties of cementitious composites. In most cases, the results acquired in different laboratories[23–26] cannot be directly compared due to significant differences in the geometry and size of the samples, the water-saturation level of the composites, the employed electrodes' material, shape and layout as well as the measurement method and the applied voltage and, if applicable, frequency. The overwhelming majority of studies involve the use of 2-probe or 4-probe direct current-based (DC) resistivity measurements.[5,10] Nevertheless, DC measurements suffer from the electrical polarization due to the movement and aggregation of the ions and, in case of 2-probe measurements, also from the lack of a clear distinction between the resistivity of a material and the contact resistance of electrode-specimen interface. To address the polarization issue, a DC field should be applied to the sample before the actual measurement to attain its full polarization. Noteworthy, the time required for the full polarization increases significantly together with the size of the element, thus limiting the industrial scale applications of this method.[5,10] Importantly, the use of alternating current (AC) methods makes it possible to overcome the polarization effect and to obtain much more stable results.[5] Moreover, while DC measurements can only record the resistivity of the entire composite simplified to a homogeneous material (usually presented as a function of functional filler content – Fig. 1a), the use of AC enables to track the formation of different solid and liquid paths within the complex microstructure of cementitious composites as well as to fully understand the variety of conduction and dielectric mechanisms occurring within cement matrix.[27,28] In particular, Electrochemical Impedance Spectroscopy (EIS) has established itself as a powerful tool for the characterization of cementitious composites' microstructure and their corrosion as well as for the investigation of the

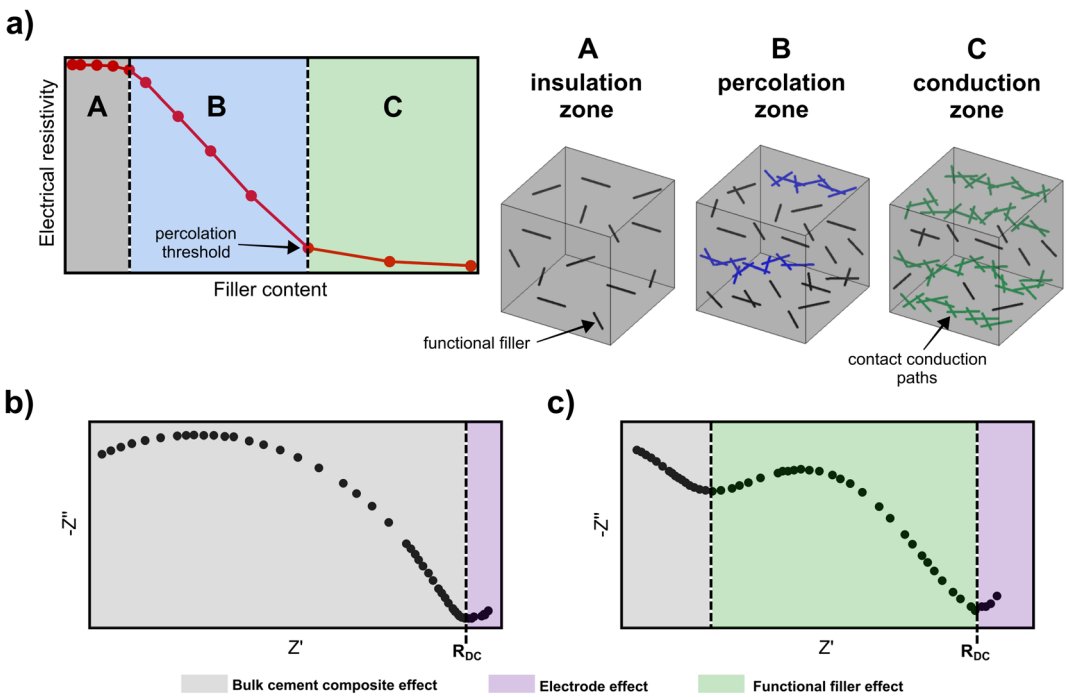

Fig. 1 Electrical properties of cementitious composites with functional fillers, *e.g.*, carbon fibres, steel fibres or CNTs: (a) the relation between the filler content and the electrical resistivity of a cementitious composite; (b) and (c) typical Nyquist plots for (b) plain cementitious composites and (c) cementitious composites with functional filler (R_{DC} represents the resistivity of the composite measured with direct current).

electrical behaviour of composites incorporating functional fillers.[27–29] EIS enables to monitor the formation of conductive paths of functional fillers reflecting their effect within intermediate frequency range on Nyquist plot (Fig. 1b and c).[30] Moreover, through impedance spectroscopy measurements one can determine the cusp point that corresponds to the DC resistance (R_{DC}) of a composite.[30] Importantly, this value is strongly influenced by the properties of cement matrix and cannot fully characterize the effect of the functional filler. Nevertheless, the high complexity of multiphase concrete microstructure as well as the high level of divergence in the experimental protocols hinder the clear understanding of the physical meaning of the impedance results gathered on cementitious composites, ultimately rendering extremely difficult the prediction of the materials' electrical response to stress and strain. Therefore, the development of novel measurement protocols to precisely monitor the formation of functional filler percolation paths within cementitious composites is a mandatory step for the application of self-sensing cementitious composites in real structures.

Here we present a novel, multifunctional cementitious composite containing electrochemically exfoliated graphene (EEG). We first manufactured cement mortars incorporating different loadings of EEG, up to 0.8 wt%, by using commercially available poly(carboxylate ether)-based superplasticizer as a surfactant to disperse graphene-based material in distilled water. We then investigated the effect of high dosages of EEG on the mechanical properties and microstructural characteristics of representative cementitious composites by investigating reference mortar and mortars incorporating 0.4 wt% and 0.6 wt% of EEG which were chosen based on the potential electrical performance, cost-effectiveness and proper workability. Finally, we performed for the first time the comprehensive electrochemical impedance spectroscopy study of oven-dried hardened EEG-based cement mortars. Based on previously reported models[31,32] as well as our previous study,[33] we developed an unprecedented, modified equivalent electrical circuit for modelling cementitious composites incorporating high loading of EEG, above the percolation threshold. The increasing loading of EEG determined a significant change of the shape of Nyquist plots when compared with plain composites. Moreover, we found that at EEG loading of 0.8 wt% all solid cement capacitive paths were replaced by EEG-based conductive paths and/or EEG-cement-EEG capacitive paths. Our findings represent an important step forward towards the wide application of EEG-based composites in self-sensing concrete structures.

Experimental

Materials

Cement, sand, distilled water, superplasticizer and graphene were used within this study to fabricate standard cement mortar according to PN-EN 196-1:2016.[34] Portland cement CEM I 42.5R was supplied by Gorażdże Cement S.A. Standard sand was purchased from Kwarcmix, while poly(carboxylate ether)-based superplasticizer (PCE) 6681F was supplied by BASF. Graphene was obtained by electrochemical exfoliation of graphite foil (Alfa Aesar, 0.5 mm thick) using a platinum wire (GoodFellow, diameter of 0.5 mm) and aqueous solution of ammonium sulfate $(NH_4)_2SO_4$ (Alfa Aesar). Mesh electrodes were soldered using copper wire or stainless-steel wire supplied by GoodFellow, both with diameter of 1 mm.

EEG synthesis and characterization

EEG was obtained by electrochemical exfoliation of graphite foil.[16,18] Graphite foil cut into pieces of *ca*. 2 cm × 2 cm served as an anode and platinum wire as a cathode in an electrolytic cell filled with aqueous solution of $(NH_4)_2SO_4$ with a concentration of 0.1 M. The voltage of 15 V was applied to start the exfoliation generating a current of *ca*. 0.4 A. The exfoliation was conducted for *ca*. 6 h. The resulting material was then sonicated and rinsed several times with water. Finally, collected graphene was immersed in liquid nitrogen for a few minutes and then freeze-dried for at least 48 h. The compositional characterization was performed with a Thermo Scientific K-Alpha X-ray photoelectron spectrometer equipped with an aluminum X-ray source (energy 1.4866 keV) at a vacuum level of 10^{-8}–10^{-9} mbar in the main chamber was used. The spot size of the X-ray beam was fixed at 400 μm.

EEG dispersion and cement mortar preparation

The aqueous dispersion of EEG with the concentration of 20 mg ml^{-1} was prepared using poly(carboxylate ether)-based superplasticizer as a surfactant. Noteworthy, PCE superplasticizers are the most commonly adopted surfactants used for dispersing graphene-based materials within cement matrix. On the one hand, PCE provides the steric repulsion and the steric hindrance effect separating graphene nanosheets from each other and from charged ions.[35,36] On the other hand, PCE products are water-reducing and workability-improving admixtures compatible with concrete. An EEG-to-surfactant ratio equivalent to 2 was employed. Superplasticizer was first dissolved in water by sonication. After adding graphene, the dispersion was then sonicated for 30 min. The cement mortar was prepared within this study following the protocol of PN-EN 196-1:2016.[34] The water-to-cement ratio and the sand-to-cement ratio were kept at 0.5 and 3.0, respectively, for all mixes. We fabricated six different cement mortars labelled as follows: R as reference mortar, and EEG_0.1, EEG_0.2, EEG_0.4, EEG_0.6, EEG_0.8 which contain 0.1 wt%, 0.2 wt%, 0.4 wt%, 0.6 wt% and 0.8 wt% (dosage by weight of cement) of EEG, respectively. The EEG dispersion was added to cement together with remaining water. After mixing, the fresh mortar was placed into steel moulds with the dimensions of 40 mm × 40 mm × 160 mm as well as into plastic cubic moulds with the dimension of 40 mm in two layers. Each layer was then vibrated on a vibration table for 30 s to remove the air from the mix. The specimens for electrical measurements were fabricated with embedded copper and steel electrodes. The exact geometry and layout of the electrodes is presented in following

paragraphs. The samples were then covered with polyethylene foil for 24 h. Thereafter, the specimens were demoulded and placed in water for additional 27 days. After the hardening period, the samples were tested or dried in the air and/or in the oven as described in following paragraphs.

Electrochemical impedance spectroscopy

The impedance spectroscopy analysis was performed using GWINSTEK LCR Meter 6300 with a frequency range swept from 20 Hz to 300 kHz. The measurements were conducted in two-probe layout. To establish the most reliable and efficient protocol for EIS measurements, we first investigated the effect of electrodes' material, geometry and distance as well as the effect of the applied voltage on the obtained Nyquist plots of reference mortar at the age of 28 days after 3 days of air-drying. For the electrodes' evaluation we have chosen two different electrodes' materials, *i.e.*, copper and stainless steel, five different shapes of the copper electrodes': wire, three meshes and plate (as presented in Fig. 2) as well as five various distances between the electrodes: 1 cm, 2 cm, 3 cm, 4 cm and 6 cm. The results revealed that (1) the use of stainless steel wire let to the higher dispersion of the recorded points, if compared to copper electrodes, and caused the formation of additional semi-circle being an effect of sample-electrode interactions (Fig. 3a); (2) the use of mesh electrodes, in particular "Mesh 2" and "Mesh 3", gave reliable results, simultaneously ensuring the proper compaction of cement mortar and efficient bond between the electrode and the composite (Fig. 3b); (3) the values of impedance measured for the electrodes' distance exceeding 2 cm are comparable (Fig. 3c). Moreover, the applied voltage (10 mV, 100 mV and 500 mV, Fig. 3d) proved to have a negligible effect on the obtained results. Therefore, the further impedance measurements of EEG-based cementitious composites were performed using copper electrodes "Mesh 3" with the distance of 3 cm and the voltage of 100 mV. All the samples, after the curing period of 28 days, were dried for 1 month in the air, followed by 24 h of oven-drying at 60 °C. The fitting of impedance spectra was performed using RelaxIS 3 software.

Mechanical properties tests and microstructural characterization

Mechanical properties tests according to PN-EN 196-1:2016[34] were conducted using CONTROLS PILOT Automatic Compression-Flexural Cement Tester on rectangular samples with the dimensions of 40 mm × 40 mm × 160 mm at the age of 28 days. The flexural strength was determined on three samples at a loading rate of 50 N s^{-1}, while the compressive strength tests were performed on six remaining halves of the samples at a loading rate of 2.4 kN s^{-1}.

After the mechanical strength tests, the samples were crushed into small pieces of 3–5 mm and then dried in the oven at 60 °C for 72 h to stop further hydration.

The microstructure of the hardened composites was evaluated by Scanning Electron Microscopy (SEM) imaging using FEI Dual Beam 235 with the accelerating voltage of 5 keV incident beam energy. The dried pieces of cement mortar were first glued to a support with conductive silver paste and the fracture surface was sputter-coated with a thin layer of gold.

Thermogravimetric Analysis (TGA) was performed using Mettler Toledo TGA/DSC 2 instrument. The pieces of mortar were grounded into fine powder and then filtered through a 80 μm sieve to remove coarse grains of sand. Three samples (*ca.* 15 mg) of each mortar were placed into alumina crucibles. The samples were first kept isothermally at 30 °C for 30 min and then heated from 30 °C to 1000 °C at a heating rate of 10 °C min^{-1}. The measurements were carried out under nitrogen atmosphere. Based on the TGA results, we determined the hydration degree and calcium hydroxide content in all samples. The hydration degree was calculated as:[37]

$$\alpha = (W_B/W_{B\infty}) \times 100\% \quad (1)$$

where $W_{B\infty}$ = 0.1667 corresponds to the maximum chemically bound water required for the full hydration of cement particles and W_B represents the chemically bound water in the mortar determined as follows:

$$W_B = L_{dh} + L_{dx} + 0.41 \times (L_{dc} - L_{dca}) \quad (2)$$

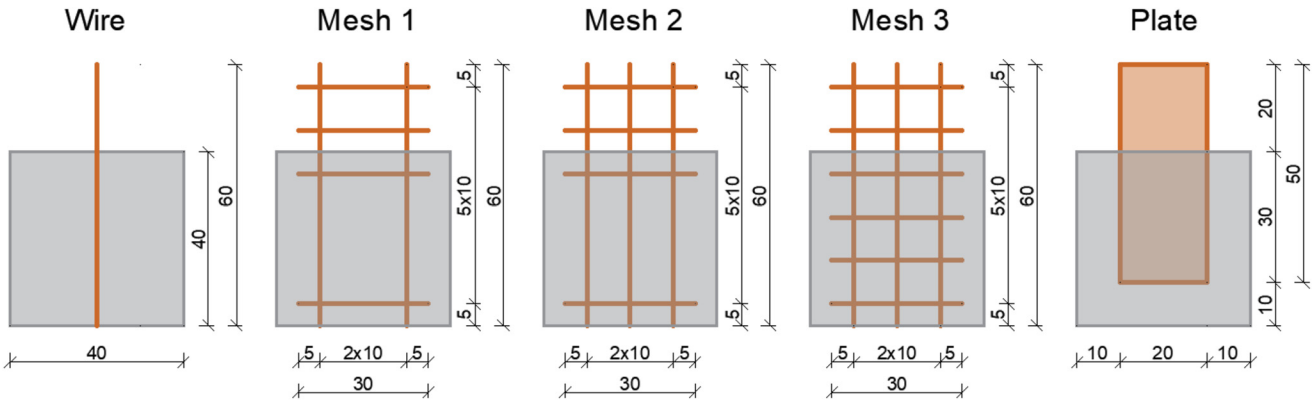

Fig. 2 The geometry of the wire, mesh and plate electrodes embedded into cement mortar samples for electrical measurements (all sizes are in mm).

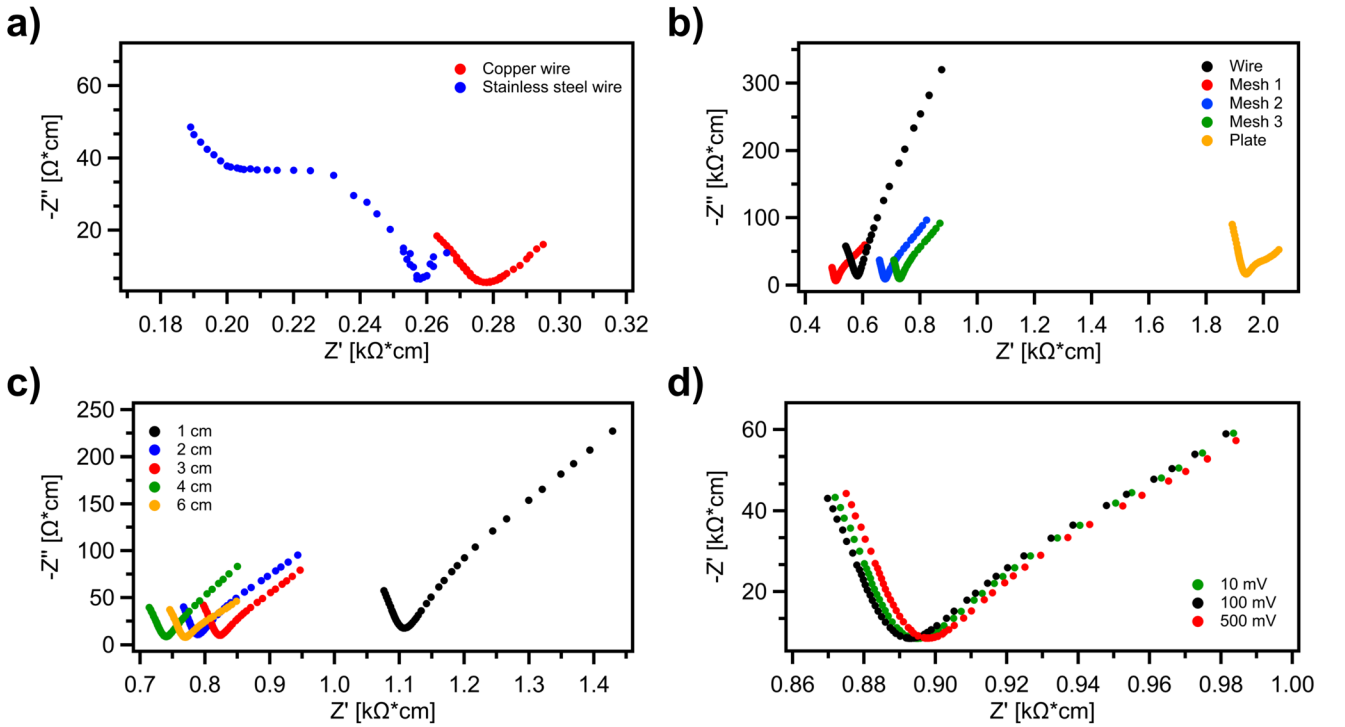

Fig. 3 Prototypical impedance spectroscopy measurements – Nyquist plots of (a) different electrodes' material, (b) different copper electrodes' shape, (c) different distance between copper electrodes, and (d) different voltage.

where L_{dh}, L_{dx}, and L_{dc} are the relative mass losses in dehydration (105–400 °C), dehydroxylation (400–530 °C) and decarbonation (530–1000 °C) regions, respectively, while L_{dca} is the subtraction of the anhydrous carbonation material in region 600–750 °C.

Results and discussion

EEG synthesis

EEG has been prepared by the electrochemical exfoliation of graphite using ammonium sulphate solution as an electrolyte, platinum wire as a cathode and graphite foil as an anode in an electrolytic cell.[16,18] Noteworthy, the electrochemical exfoliation process of graphene production holds a great technological potential, since it can be easily upscaled. The electrolysis process lasting 6 h allowed us to produce *ca.* 300 mg of dry EEG.

The lateral size of EEG sheets varies between 2 μm and 5 μm with bilayer graphene being the main product.[18] The chemical composition of the produced EEG was assessed by X-ray photoelectron spectroscopy (XPS) analyses. From the survey spectra, a C/O ratio of 6.7 is estimated for the exfoliated EEG (Fig. 4) which is typical for electrical conductive graphene-based materials.[38] To further investigate the chemical structure of EEG, we fitted the high-resolution C 1s XPS spectrum with 5 Gaussian–Lorentzian curves for the 5 functional groups: 284.4 eV C–C (C sp^2–C sp^2), 285.15 eV C–O (including C sp^2–O–C sp^2, C sp^3–OH and C sp^2–OH), 286.48 eV C–O–C (C sp^3–O–C sp^3), 287.38 eV C═O, and 288.50 eV COOR (COOH and ester) (Fig. 4). The C–C (C sp^2–C sp^2) moiety is prevailing with 62.7% of relative abundance confirming the electrically conductive structure of EEG.

Mechanical and microstructural characterization

The high loadings of nanomaterials required to obtain the percolation threshold and stable electric response of the material may lead to the formation of aggregates inhibiting the cement hydration and deteriorating the microstructure of hardened composites. Therefore, we further investigated the effect of selected EEG dosages, *i.e.*, 0.4 wt% and 0.6 wt%, on the mechanical properties, hydration degree and microstructure formation of cementitious composites at the age of 28 days.

Fig. 5a plots the results of the compressive and flexural strength tests, while Fig. 5b shows the $Ca(OH)_2$ content and hydration degree calculated on the basis of TGA measurements. On the one hand, we observed a gradual decrease in the strength of cementitious composites with the addition of high loading of EEG as quantified by 7.57 MPa and 54.61 MPa of flexural and compressive strength, respectively, for the reference mortar, up to 6.16 MPa and 43.49 MPa for EEG_0.6 mortar (attesting a decrease of 19% and 20%, respectively). On the other hand, the calcium hydroxide content increased by 11% and the hydration degree remained relatively unaltered with the addition of 0.6 wt% of EEG, if compared to the reference mortar. Even though the hydration degree of the composites remained the same for all samples, most probably

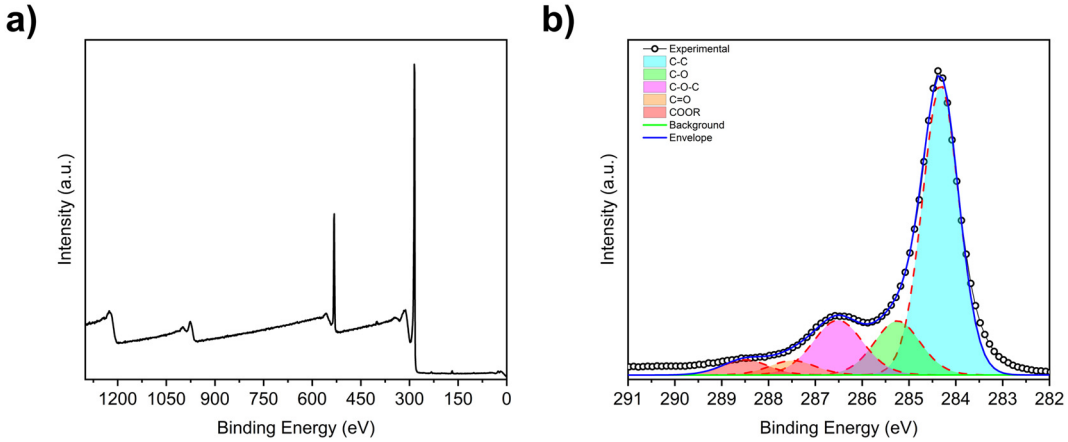

Fig. 4 (a) XPS survey; (b) High resolution XPS C 1s peak.

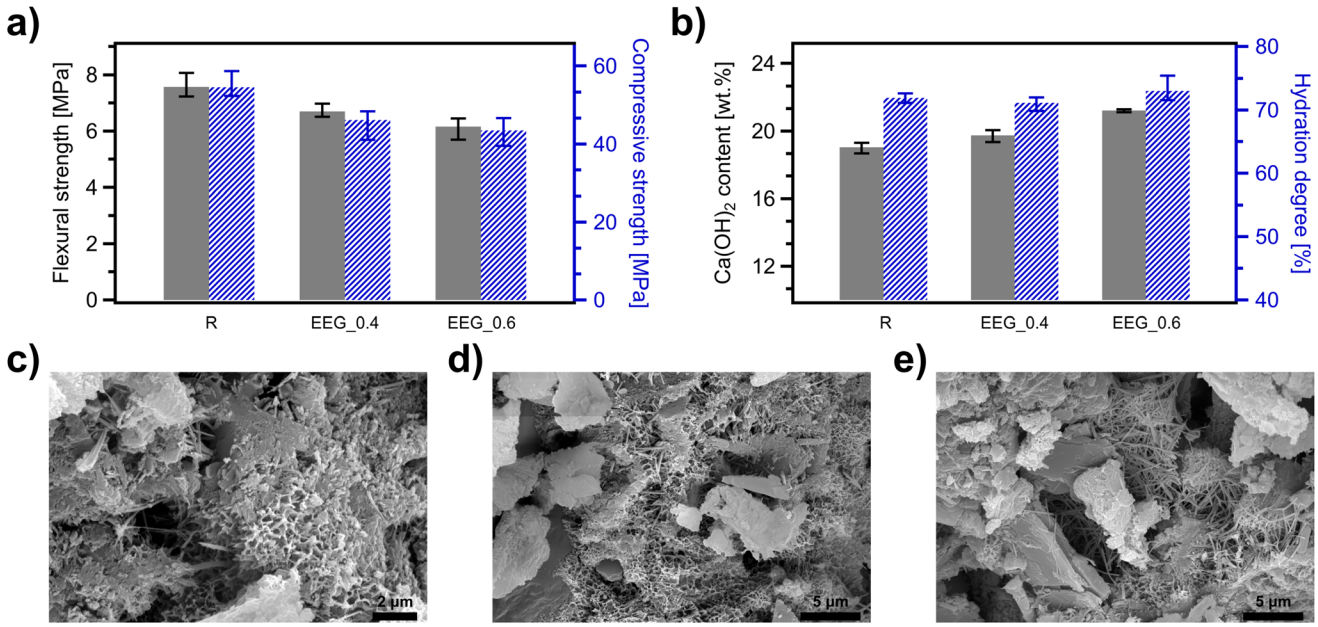

Fig. 5 Mechanical properties tests and structural characterization of R, EEG_0.4 and EEG_0.6 cement mortars at the age of 28 days: (a) compressive and flexural strength, (b) calcium hydroxide content and hydration degree, (c–e) SEM images for R, EEG_0.4 and EEG_6 mortars, respectively.

the high loading of EEG and PCE resulted in the higher porosity of hardened composites and higher formation of weaker hydration products, *i.e.*, ettringite and calcium hydroxide crystals (Fig. 5c–e).

Impedance analysis of EEG-based cementitious composites

In order to determine the effect of EEG nanosheets on the electrical performance of cementitious composites as well as to gain deep understanding of the formation of electroactive graphene-based paths within cement matrix, we performed the electrochemical impedance spectroscopy studies on hardened EEG-based cement mortars incorporating up to 0.8 wt% of EEG.

Noteworthy, the Nyquist plots of water-saturated cementitious composites are dominated mainly by the effect of the electrode-specimen interface, therefore, to fully explore the changes of the impedance occurring together with the increasing loading of EEG, we analysed the Nyquist plots for all cement mortars after 1 month of air-drying followed by 24 h of oven-drying. In general, the addition of EEG results in a substantial change of the impedance spectrum shape. While a typical semi-circle is highly visible for reference composite (Fig. 6a), the addition of EEG leads to the significant flattening of the curve by modifying the ratio between the imaginary and real part of the impedance (Fig. 6b–e). Finally, the Nyquist plot of EEG_0.8 mortar (Fig. 6f) reveals the presence of two semi-circles: similarly to composites with carbon fibres and CNTs,[30,39,40] the additional semi-circle, being a fingerprint of the EEG nanosheets presence, appeared in intermediate fre-

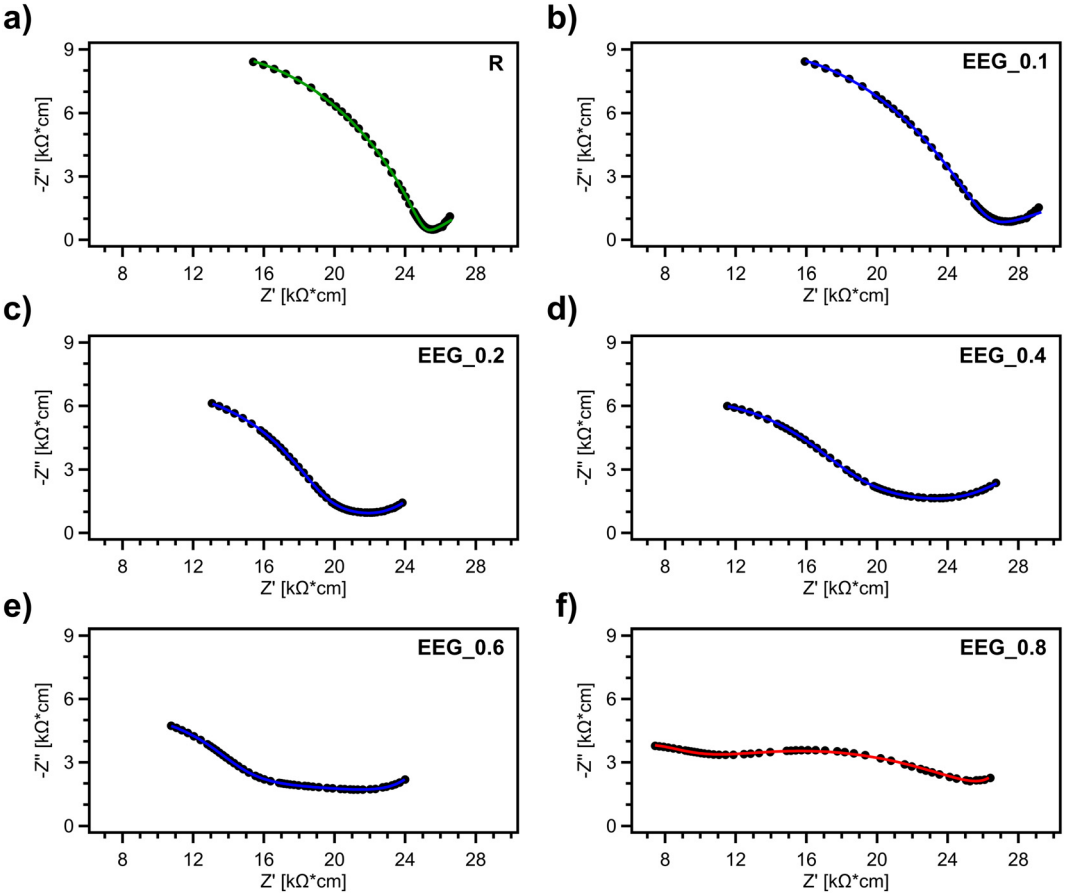

Fig. 6 Nyquist plots for mortar samples dried in the oven for 24 h: (a) reference mortar R, (b)–(f) mortars incorporating from 0.1 wt% to 0.8 wt% of EEG. Note: green, blue and red colours represent the fitting with the equivalent electrical circuits I, II and III, respectively, according to Fig. 3.

quency region. Moreover, the results indicate the notable frequency dependence of the measured resistivity. On the one hand, the resistivity measured for the frequency of 300 kHz considerably decreased with the addition of graphene: the average values of 8.76 kΩ cm and 15.47 kΩ cm were achieved for EEG_0.8 and R mortars, respectively (the decrease of 43.4%). On the other hand, even though it is highly visible that EEG strongly affects the electrical response of the cementitious composites to AC, the resistivity considered as the resistivity of the bulk cement matrix (previously labelled as R_{DC}) that can be measured within the frequency range of 30–300 Hz remained relatively unaltered in all samples.

Electrical equivalent circuit for EEG-based cementitious composites

We further processed the EIS data with the fitting procedure using the equivalent circuits reported in our previous study on rGO-based cementitious composites.[33] Within this work we established two equivalent electrical circuits: a "modified conductive paths" circuit (based on Song's circuit[31] and its modification,[41] circuit I in Fig. 7) for reference composite and a circuit with additional graphene-based paths for composites with rGO loading from 0.075 wt% to 0.2 wt% (circuit II in Fig. 7). The former involves the simulation of three conductive paths within cement matrix: the continuous conductive paths formed by uninterruptedly connected pores (modelled as a resistor R_1), the insulator paths representing the solid layers of cement hydrates (modelled as a capacitor C_1) and the discontinuous conductive paths of solid layers disrupted locally by pores (modelled as a constant phase element CPE_1). The latter introduces an additional circuit consisting of continuous conductive graphene-based paths (modelled as a resistor R_2) and capacitive paths formed by solid cement matrix layers between graphene nanosheets (modelled as a capacitor C_2). For each of them the electrode-specimen interface was represented by an additional constant phase element CPE_e. All the fitted spectra are presented together with the experimental curves in Fig. 5. Importantly, the proposed circuits mimicked efficiently the experimental results for reference mortar (circuit I) and mortars with EGG loading up to 0.6 wt% (circuit II). Nevertheless, the use of circuit II for fitting the EEG_0.8 led to high fitting errors, in particular within the insulator paths of cement matrix indicating that the value of C_1 is close to zero. This is most probably due to the increasing loading of EEG leading to the disappearance of the insulator paths of cement matrix, *i.e.*, all the paths of solid layers of cement hydrates

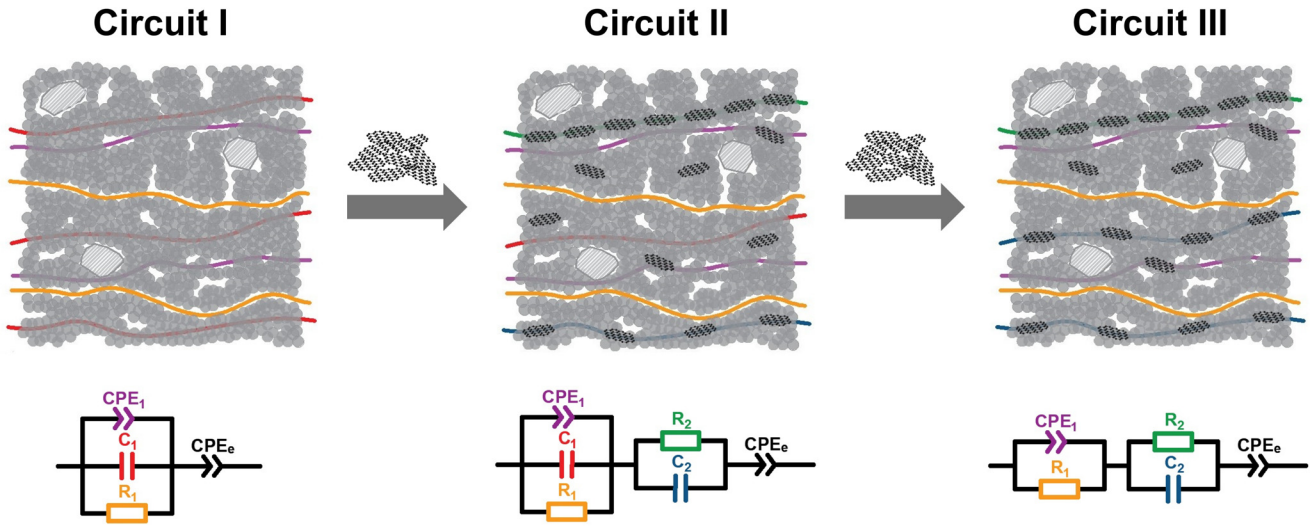

Fig. 7 Equivalent electrical circuits applied for the fitting of electrochemical impedance spectroscopy results of EEG-based cement mortars: circuit I – reference mortar, circuit II – mortars with EEG loading from 0.1 wt% to 0.6 wt%, circuit III – mortar with 0.8 wt% loading of EEG (description in the text).

transform into capacitive EEG-cement-EEG paths. Therefore, we have proposed a new equivalent circuit for cementitious composites incorporating high loadings of EEG (circuit III in Fig. 7) by removing C_1 capacitor.

Fig. 8 displays the key performance indicators of equivalent electrical circuits for oven-dried reference and EEG-based composites. It is worth pointing out that the first addition of EEG, *i.e.*, 0.1 wt%, results in the notable drop of the R_1 resistivity, from 25.01 kΩ cm to 16.17 kΩ cm, if compared to reference mortar. This observation can be explained by the addition of PCE superplasticizer to EEG dispersion. Within our previous study on rGO based composites,[28] we reported the reduction

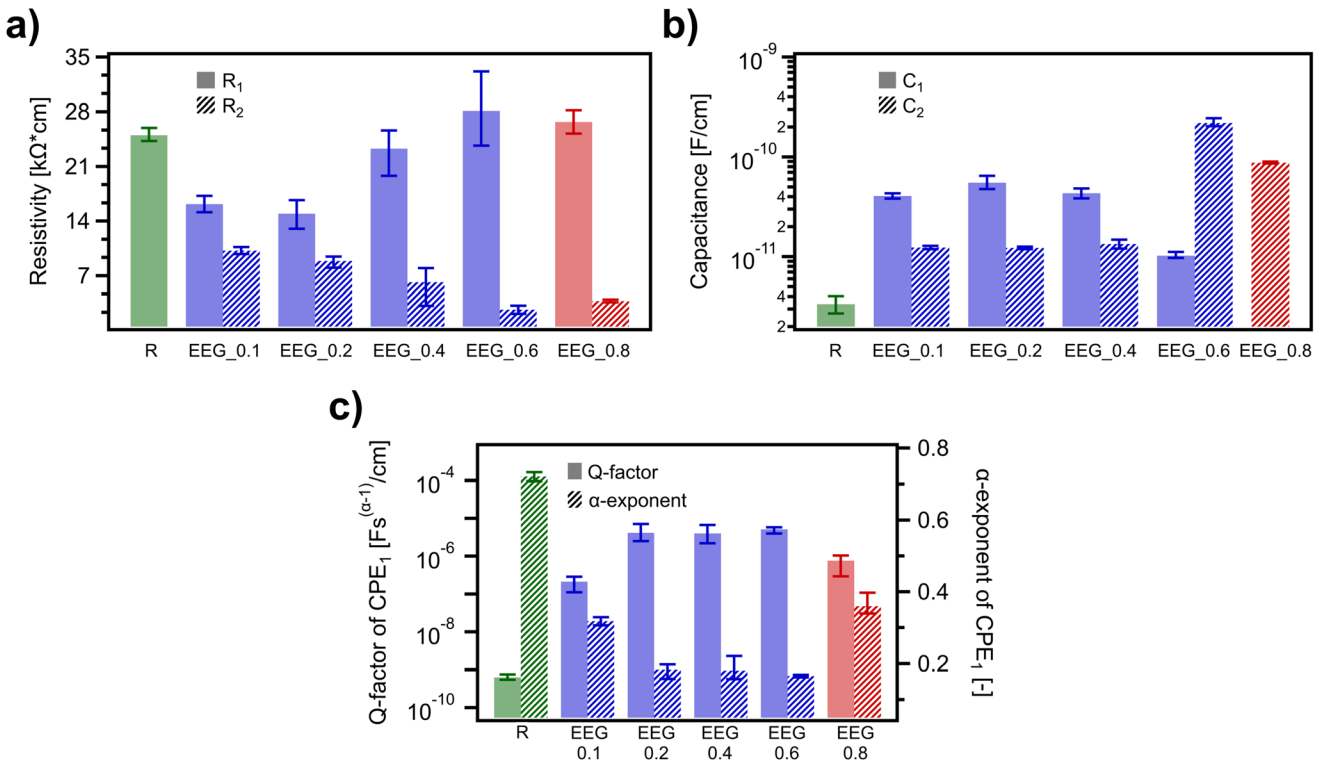

Fig. 8 Values of the equivalent circuit components for all mortars, oven-dried for 24 h: (a) R_1 and R_2, (b) C_1 and C_2, (c) Q-factor and α-exponent of CPE_1. Note: the values of the components of the equivalent circuits are normalized on the basis of the samples' geometry and the distance between the electrodes.

of R_1 for composites with the addition of PCE due to the higher porosity of the mortars. Nevertheless, the further increase of EEG dosage from 0.1 wt% to 0.6 wt% is accompanied by an increase of R_1 resistivity and a reduction of R_2 resistivity (Fig. 8a). The increase of the resistivity of the continuous conductive paths of cement matrix can be attributed to the higher hydration degree of EEG-based mortars that was further confirmed in microstructural characterization. The reduction of R_2 resistivity confirms the formation of higher number of graphene-based conductive paths within the composite. Initially, the changes of capacitance are inversely proportional to the changes of the resistivity (Fig. 8b). The higher porosity determines a significant increase of C_1 capacitance from 3.35×10^{-12} F cm^{-1} to 4.08×10^{-11} F cm^{-1} with the EEG addition of 0.1 wt%. Interestingly, further increase of EEG loading up to 0.4 wt% results in the negligible difference in both C_1 and C_2 values. This can be attributed to the fact that the increasing hydration degree combined with higher loading of EEG should decrease the capacitance C_1 of cement matrix and increase the capacitance C_2 of EEG-cement-EEG paths. Nevertheless, since the EEG loading up to 0.4 wt% is too low to reach the percolation threshold, the minor changes in the formation of C_1 and C_2 paths cannot be detected. Noteworthy, the addition of 0.6 wt% of EEG leads to a decrease of the C_1 capacitance to 1.02×10^{-11} F cm^{-1}, simultaneously increasing C_2 capacitance, achieving value as high as 2.20×10^{-10} F cm^{-1} (the increase from 1.34×10^{-11} F cm^{-1} observed for EEG_0.4 mortar), being an effect of the reduced distance between EEG nanosheets. Finally, as described before, the dosage of 0.8 wt% of EEG favours the replacement of all cement insulator paths with EEG-cement-EEG capacitor paths. Moreover, the value of C_2 capacitance starts to decrease with 0.8 wt% loading of EEG content indicating the initiation of contact conduction precluding the further storage of electric charge. The values of the Q-factor and the α-exponent of CPE_1 (Fig. 8c) follow a similar trend to the resistivity and capacitance plots further confirming the changes in porosity of the composites as well as the increasing number of randomly embedded EEG nanosheets along the discontinuous conductive paths of cement mortar. The results above taken together suggest that the loading of 0.8 wt% can be considered as a percolation threshold for EEG cementitious composites.

Conclusions

In summary, we have developed a novel EEG-based cementitious composites featuring on-demand electrical characteristics. We first manufactured 6 types of cement mortars upon gradually adding up to 0.8 wt% of EEG. The use of such EEG load without the occurrence of aggregation of segregation between the components was possible thanks to the incorporation of a PCE superplasticizer as a surfactant ensuring optimal EEG aqueous dispersion. We applied electrochemical impedance spectroscopy to investigate the electrical properties and conduction mechanisms of EEG-based cement mortars. The comprehensive EIS study was conducted within the frequency range from 20 Hz to 300 kHz on oven-dried samples. The results obtained allow to gain a full picture of the electroactive network of EEG assemblies generated within cement matrix. We found the formation of EEG-based percolation paths even in samples with relatively low EEG dosages. Moreover, the addition of 0.8 wt% of EEG significantly modified the electrical response of the material to the AC field, if compared with plain cement mortar, making it possible to propose for the first time a new, modified electrical equivalent circuit for modelling cementitious composites with EEG loadings exceeding percolation threshold. Our findings mark a significant advancement in the field of Structural Health Monitoring through the development of unprecedented, efficient, and reliable protocol for the measurement of electrical properties of self-sensing composites, paving the way towards a wide range of applications of EEG-based composites in self-sensing structures. Overall, this study offers a novel powerful nanoscale strategy for the monitoring of the electrical properties of cementitious composites, opening up new avenues towards meeting the increasing demand of SHM applications.

Author contributions

The manuscript was written through contributions of all authors. All authors have given approval to the final version of the manuscript.

Data availability

Original data are available upon request to be sent to the corresponding author of the paper.

Conflicts of interest

There are no conflicts to declare.

Acknowledgements

We acknowledge financial support from the Polish National Science Center (Grant No. 2019/33/N/ST5/00832), the Silesian University of Technology with Statutory Founds of Department of Structural Engineering (grant agreement BK-230/RB6/2024), the European Commission through the ERC project SUPRA2DMAT (GA-833707) and the HORIZON-CL4-2023-DIGITAL-EMERGING-01-CNECT project 2D-PRINTABLE (GA-101135196) as well as the Agence Nationale de la Recherche through the Interdisciplinary Thematic Institute SysChem *via* the IdEx Unistra (ANR-10-IDEX-0002) within the program Investissement d'Avenir, the Foundation Jean-Marie Lehn and the Institut Universitaire de France (IUF) and the University of Strasbourg Institute for Advanced Study (USIAS).

References

1 M. J. Hanus and A. T. Harris, *Prog. Mater. Sci.*, 2013, **58**, 1056–1102.
2 S. Ding, X. Wang, L. Qiu, Y.-Q. Ni, X. Dong, Y. Cui, A. Ashhour, B. Han and J. Ou, *Small*, 2023, **19**, 2206258.
3 Z. Tian, Y. Li, J. Zheng and S. Wang, *Composites, Part B*, 2019, **177**, 107437.
4 S. Ding, Y. Xiang, Y.-Q. Ni, V. K. Thakur, X. Wang, B. Han and J. Ou, *Nanotoday*, 2022, **43**, 101438.
5 B. Han, X. Yu, J. Ou, B. Han, X. Yu and J. Ou, in *Self-Sensing Concrete in Smart Structures*, Elsevier, 2014, pp. 67–93.
6 J. Lee, S. Mahendra and P. J. J. Alvarez, *ACS Nano*, 2010, **4**, 3580–3590.
7 D. Lu, L.-P. Ma, J. Zhong, J. Tong, Z. Liu, W. Ren and H.-M. Cheng, *ACS Nano*, 2023, **17**, 3587–3597.
8 B. Funk, D. Göhler, B. Sachsenhauser, M. Stintz, B. Stahlmecke, B. A. Johnson and W. Wohlleben, *Environ. Sci.: Nano*, 2019, **6**, 1443.
9 B. Han, X. Yu, J. Ou, B. Han, X. Yu and J. Ou, in *Self-Sensing Concrete in Smart Structures*, Elsevier, 2014, pp. 189–230.
10 B. Han, S. Ding and X. Yu, *Measurement*, 2015, **59**, 110–128.
11 B. Han, X. Yu, J. Ou, B. Han, X. Yu and J. Ou, in *Self-Sensing Concrete in Smart Structures*, Elsevier, 2014, pp. 361–376.
12 A. M. Rashad, *Constr. Build. Mater.*, 2017, **153**, 81–101.
13 W. Wang, S. J. Chen, F. B. de Souza, B. Wu and W. H. Duan, *Nanoscale*, 2018, **10**, 1004–1014.
14 K. S. Novoselov, A. K. Geim, S. V. Morozov, D. Jiang, Y. Zhang, S. V. Dubonos, I. V. Grigorieva and A. A. Firsov, *Science*, 2004, **306**, 666–669.
15 A. K. Geim and K. S. Novoselov, *Nat. Mater.*, 2007, **6**, 183–191.
16 M. Eredia, S. Bertolazzi, T. Leydecker, M. El Garah, I. Janica, G. Melinte, O. Ersen, A. Ciesielski and P. Samorì, *J. Phys. Chem. Lett.*, 2017, **8**, 3347–3355.
17 S. Yang, M. R. Lohe, K. Müllen and X. Feng, *Adv. Mater.*, 2016, **28**, 6213–6221.
18 M. Krystek, D. Pakulski, V. Patroniak, M. Górski, L. Szojda, A. Ciesielski and P. Samorì, *Adv. Sci.*, 2019, **6**, 1801195.
19 M. Krystek, D. Pakulski, M. Górski, L. Szojda, A. Ciesielski and P. Samorì, *ACS Appl. Mater. Interfaces*, 2021, **13**, 23000–23010.
20 K. Parvez, Z. Wu, R. Li, X. Liu, R. Graf, X. Feng and K. Müllen, *J. Am. Chem. Soc.*, 2014, **136**, 6083–6091.
21 M. Du, H. Jing, Y. Gao, H. Su and H. Fang, *Nanotechnol. Rev.*, 2020, **9**, 115–135.
22 Y. Lin and H. Du, *Constr. Build. Mater.*, 2020, **265**, 120312.
23 J.-L. Le, H. Du and S. D. Pang, *Composites, Part B*, 2014, **67**, 555–563.
24 J. Tao, X. Wang, Z. Wang and Q. Zeng, *Constr. Build. Mater.*, 2019, **209**, 665–678.
25 Q. Liu, Q. Xu, Q. Yu, R. Gao and T. Tong, *Constr. Build. Mater.*, 2016, **127**, 565–576.
26 Q. Liu, W. Wu, J. Xiao, Y. Tian, J. Chen and A. Singh, *Constr. Build. Mater.*, 2019, **208**, 482–491.
27 X. Hu, C. Shi, X. Liu, J. Zhang and G. De Schutter, *Cem. Concr. Compos.*, 2019, **100**, 1–14.
28 W. Pichór, M. Frąc and M. Radecka, *Cem. Concr. Compos.*, 2022, **125**, 104328.
29 H. Wang, A. Zhang, L. Zhang, Q. Wang, X. Yang, X. Gao and F. Shi, *Constr. Build. Mater.*, 2020, **265**, 120740.
30 J. Zhang, A. Heath, H. M. T. Abdalgadir, R. J. Ball and K. Paine, *Constr. Build. Mater.*, 2022, **353**, 129049.
31 G. Song, *Cem. Concr. Res.*, 2000, **30**, 1723–1730.
32 J. M. Cruz, I. C. Fita, L. Soriano, J. Payá and M. V. Borrachero, *Cem. Concr. Res.*, 2013, **50**, 51–61.
33 M. Safuta, A. Ciesielski and P. Samorì, *Chem. – Eur. J.*, 2023, **29**, e2023018.
34 PN-EN 196-1:2016 – Metody badania cementu – Część 1: Oznaczanie wytrzymałości.
35 Z. Lu, A. Hanif, C. Ning, H. Shao, R. Yin and Z. Li, *Mater. Des.*, 2017, **127**, 154–161.
36 L. Zhao, X. Guo, C. Ge, Q. Li, L. Guo, X. Shu and J. Liu, *Composites, Part B*, 2017, **113**, 308–316.
37 S. M. Monteagudo, A. Moragues, J. C. Gálvez, M. J. Casati and E. Reyes, *Thermochim. Acta*, 2014, **592**, 37–51.
38 C. Valentini, V. Montes-García, P. A. Livio, T. Chudziak, J. Raya, A. Ciesielski and P. Samorì, *Nanoscale*, 2023, **15**, 5743–5755.
39 T. O. Mason, M. A. Campo, A. D. Hixson and L. Y. Woo, *Cem. Concr. Compos.*, 2002, **24**, 457–465.
40 S. Wansom, N. J. Kidner, L. Y. Woo and T. O. Mason, *Cem. Concr. Compos.*, 2006, **28**, 509–519.
41 J. M. Cruz, I. C. Fita, L. Soriano, J. Payá and M. V. Borrachero, *Cem. Concr. Res.*, 2013, **50**, 51–61.